INTERNATIONAL JOURNAL FOR NUMERICAL METHODS IN FLUIDS
Int. J. Numer. Meth. Fluids 2000; **34**: 425–448

A reduced-order approach for optimal control of fluids using proper orthogonal decomposition

S. S. Ravindran*,[1]

Department of Mathematical Sciences, University of Alabama in Huntsville, Huntsville, AL, U.S.A.

SUMMARY

In this article, a *reduced-order modeling* approach, suitable for active control of fluid dynamical systems, based on proper orthogonal decomposition (POD) is presented. The rationale behind the reduced-order modeling is that numerical simulation of Navier–Stokes equations is still too costly for the purpose of optimization and control of unsteady flows. The possibility of obtaining reduced-order models that reduce the computational complexity associated with the Navier–Stokes equations is examined while capturing the essential dynamics by using the POD. The POD allows the extraction of a reduced set of basis functions, perhaps just a few, from a computational or experimental database through an eigenvalue analysis. The solution is then obtained as a linear combination of this reduced set of basis functions by means of Galerkin projection. This makes it attractive for optimal control and estimation of systems governed by partial differential equations (PDEs). It is used here in active control of fluid flows governed by the Navier–Stokes equations. In particular, flow over a backward-facing step is considered. Reduced-order models/low-dimensional dynamical models for this system are obtained using POD basis functions (global) from the finite element discretizations of the Navier–Stokes equations. Their effectiveness in flow control applications is shown on a recirculation control problem using blowing on the channel boundary. Implementational issues are discussed and numerical experiments are presented. Copyright © 2000 John Wiley & Sons, Ltd.

KEY WORDS: flow control; Galerkin approximation; optimal control; POD; reduced-order model

1. INTRODUCTION

The invention of micro-electromechanical systems and other fast micro-devices has generated substantial interest in active control of fluid dynamical systems for the design of advanced fluid dynamic technology. There is a lot of literature devoted to this actively growing field. For example, in References [1–6,28], various control problems in viscous incompressible flows were discussed. In References [7–11], experimental efforts were reported. However, efficient

* Correspondence to: Department of Mathematical Sciences, University of Alabama in Huntsville, Huntsville, AL 35899, U.S.A.
[1] E-mail: ravindra@ultra.math.uah.edu www.math.uah.edu/ravindra

Received 10 October 1999
Revised 25 January 2000

computational methodologies for use in on-line, real-time computations for partial differential equation (PDE) based control design has seen little progress. In this article we discuss a reduced-order method for PDE-based control using the proper orthogonal decomposition (POD).

The solution of complex fluid dynamic equations using the available finite element, finite volume, finite difference or spectral methods is, in general, not feasible for real-time estimation and control. There are methods that would yield small degree-of-freedom models for the purpose of control of PDEs. However, they do not adequately represent the physics of the system and may be very sensitive to operating conditions, as they are based on input/output data of a given system.

We examine the possibility of obtaining reduced-order models that reduce the computational complexity associated with the Navier–Stokes equations while capturing the essential dynamics by using the POD. The POD is a model reduction technique for complex non-linear problems. It was first proposed by Karhunen [12] and Loeve [13], independently, and is sometimes called the Karhunen–Loeve (K–L) expansion. Subsequently, it has been applied in various applications. In Reference [14], the method was first called POD and it was used to study turbulent flows. In Reference [15] another important progress was made and the method of 'snapshots' was incorporated into the POD framework, which will be described in the sequel to this paper. Other applications in turbulent flow simulations are given in References [16–22].

When discretizing non-linear PDEs using finite volume, finite difference, finite element or spectral methods, one uses basis functions that have very little connection with the problem or with the underlying PDEs. In some spectral methods, Legendre polynomials are used; in finite element methods, piecewise polynomials are used and in finite difference methods, grid functions are used. However, the POD uses basis functions that are generated from the numerical solutions of the system or from the experimental measurements.

The essential idea is to generate a reduced set of basis functions for Galerkin representations of PDEs. In other words, given an ensemble $\mathscr{S} = \{\mathbf{U}^{(i)}\}_{i=1}^{N}$, consisting of N data vectors of length N_x, the POD theory yields that we can find an orthonormal co-ordinate system $\{\mathbf{V}^{(i)}\}_{i=1}^{N_x}$ such that the variance of the dataset in the co-ordinate directions becomes maximal. Thus, when the Navier–Stokes equations are projected onto this base using a Galerkin projection, one obtains a reduced-order model. The beauty of the POD is that it is a non-linear model reduction approach and its mathematical theory is based on the spectral theory of compact, self-adjoint operators.

Our goals here are first to apply the POD to simulate flow over a backward-facing step in a two-dimensional channel; second, to apply the POD to an optimal control problem for this configuration. Backward-facing step flow serves as a prototype for unsteady separated flow. For high Reynolds numbers, the flow separates near the corner of the step and recirculation appears downstream of the step. Such recirculation regions will strongly influence heat and mass transfer [23]. We will formulate and numerically solve a recirculation control problem in this configuration with the control action achieved through blowing of mass on a part of the boundary.

The layout of the paper is as follows. In the remainder of this section we establish the notation that will be used throughout the paper. In Section 2 we present the POD and its properties. In Section 3 we present numerical simulations of the channel flow using a finite

element method and compare it with POD reduced-order model solutions. In Section 4 we formulate an optimal control problem in this configuration and apply the POD to derive a reduced-order optimal control problem. We will also describe a numerical procedure to solve such an optimal control problem. In Section 5 we present computational results for the optimal control problem and we conclude the paper with Section 6.

1.1. Notations

We denote by $L^2(\Omega)$ the collection of square-integrable functions defined on flow region $\Omega \subset \mathbb{R}^2$ and we denote the associated norm by $\|\cdot\|_0$. Let $H_1(\Omega) = \{v \in L^2(\Omega)$: $\partial v/\partial x_i \in L^2(\Omega)$, for $i = 1, 2\}$ and the norm on it be $\|\cdot\|_1$. We denote by $L^2(0, T; H^1)$ the space of all measurable functions f: $(0, T) \to H^1$ such that $\|f\|_{L^2(0,T;\,H^1)} = (\int_0^T \|f\|_1^2 \, dt)^{1/2} < \infty$. Vector-valued counterparts of these spaces are denoted by boldface symbols, e.g., $\mathbf{H}^1(\Omega) = [H^1(\Omega)]^2$. The $L^2(\Omega)$ or $\mathbf{L}^2(\Omega)$ inner product is denoted by $(\cdot, \cdot)$.

2. THE POD SUB-SPACE

In order to illustrate the POD reduced basis sub-space and its construction, we assume for ease of exposition that we are dealing with the semi-discrete non-linear problem

$$\frac{d\mathbf{y}}{dt} = \mathscr{E}(\mathbf{y}, t), \qquad t \in \mathbb{R}, \quad \mathbf{y} \in \mathbf{X}$$

where $\mathbf{X}$ is a finite-dimensional space. If the finite element method were used to solve the above semi-discrete problem, $\mathbf{X}$ would be a piecewise polynomial space. However, the choice for the POD reduced basis sub-space is different.

2.1. The POD

The underlying problem is to identify a structure in an ensemble of vector fields. Given an ensemble of vector fields $\mathbf{U}^{(i)}$, we seek to find a function $\mathbf{\Phi}$, which has a structure typical of the members of the ensemble. One way to resolve the problem is to project the ensemble on $\mathbf{\Phi}$, i.e., $(\mathbf{U}^{(i)}, \mathbf{\Phi})$, to find $\mathbf{\Phi}$, which is as nearly parallel as possible. Thus, we want to maximize $(\mathbf{U}^{(i)}, \mathbf{\Phi})$ while removing the amplitude by normalizing it. It is now natural to look at a space of functions $\mathbf{\Phi}$ for which the inner-product $(\mathbf{\Phi}, \mathbf{\Phi})$ exists, i.e., $\mathbf{\Phi}$ must be $L^2(\Omega)$. In order to include the statistics, we must maximize the expression

$$\frac{(\mathbf{\Phi}, \mathbf{U}^{(i)})}{(\mathbf{\Phi}, \mathbf{\Phi})^{1/2}}$$

in some average sense. Furthermore, as we are only interested in magnitude and not the sign, we consider the mean of the square of the expression. That is, given an ensemble set

$$\mathscr{S} = \{\mathbf{U}^{(i)}\colon\ 1 \le i \le N\}$$

seek a function $\mathbf{\Phi} \in \mathbf{L}^2(\Omega)$, which gives the best representation of $\mathscr{S}$ in the sense that it maximizes

$$\frac{1}{N} \sum_{i=1}^{N} \frac{|(\mathbf{U}^{(i)}, \mathbf{\Psi})|^2}{(\mathbf{\Psi}, \mathbf{\Psi})} \tag{2.1}$$

In other words, one seeks a function that has the largest mean square projection on the set $\mathscr{S}$. The maximization problem (2.1) can be cast in an equivalent eigenvalue problem. To see this, define

$$\mathbf{K}\mathbf{\Phi} = \frac{1}{N} \sum_{i=1}^{N} \int_{\Omega} \mathbf{U}^{(i)}(\mathbf{x}) \mathbf{U}^{(i)}(\mathbf{x}') \mathbf{\Phi}(\mathbf{x}') \, \mathrm{d}\mathbf{x}' \tag{2.2}$$

then

$$(\mathbf{K}\mathbf{\Phi}, \mathbf{\Phi}) = \frac{1}{N} \sum_{i=1}^{N} \int_{\Omega} \int_{\Omega} \mathbf{U}^{(i)}(\mathbf{x}) \mathbf{\Phi}(\mathbf{x}) \mathbf{U}^{(i)}(\mathbf{x}') \mathbf{\Phi}(\mathbf{x}') \, \mathrm{d}\mathbf{x} \, \mathrm{d}\mathbf{x}' = \frac{1}{N} \sum_{i=1}^{N} |(\mathbf{U}^{(i)}, \mathbf{\Phi})|^2$$

Moreover, we have

$$\frac{(\mathbf{K}\mathbf{\Phi}, \mathbf{\Phi})}{(\mathbf{\Phi}, \mathbf{\Phi})} = \frac{\frac{1}{N} \sum_{i=1}^{N} |(\mathbf{U}^{(i)}, \mathbf{\Phi})|^2}{(\mathbf{\Phi}, \mathbf{\Phi})} = \lambda$$

Using the calculus of variations, we can find the maximum, as described below. Let ϕ^* be a function that maximizes λ. We can then write any other function as $\phi^* + \epsilon\phi'$. Then λ can be written as

$$F(\epsilon) = \frac{(\mathbf{K}\mathbf{\Phi}^*, \mathbf{\Phi}^*) + \epsilon(\mathbf{K}\mathbf{\Phi}', \mathbf{\Phi}') + \epsilon(\mathbf{K}\mathbf{\Phi}', \mathbf{\Phi}^*) + \epsilon^2(\mathbf{K}\mathbf{\Phi}', \mathbf{\Phi}')}{(\mathbf{\Phi}^*, \mathbf{\Phi}^*) + \epsilon(\mathbf{\Phi}^*, \mathbf{\Phi}') + \epsilon(\mathbf{\Phi}', \mathbf{\Phi}^*) + \epsilon^2(\mathbf{\Phi}', \mathbf{\Phi}')} = \lambda$$

Clearly, the maximum occurs when $\epsilon = 0$ and thus $(\mathrm{d}F(\epsilon)/\mathrm{d}\epsilon)\big|_{\epsilon=0} = 0$. This leads one to

$$(\mathbf{K}\mathbf{\Phi}^*, \mathbf{\Phi}') = \lambda(\mathbf{\Phi}^*, \mathbf{\Phi}')$$

It is now clear that the maximization problem (2.1) is the same as finding the eigenvalue of the eigenvalue problem

$$\mathbf{K}\mathbf{\Phi}^* = \lambda\mathbf{\Phi}^* \tag{2.3}$$

For practical calculations, the number of grid points N can be rather large, leading to a very large eigenvalue problem. In order to save time in the computation of the eigenfunction, a useful method was proposed in Reference [15], where it was called the *method of snapshots*. The steps involved in the method axe first to take the ensemble set

$$\mathscr{S} = \{\mathbf{U}^{(i)}: 1 \le i \le N\}$$

as solutions at N different time steps t_i. Second to assume $\mathbf{\Phi}$ has a special form in terms of the original data as

$$\mathbf{\Phi} = \sum_{i=1}^{N} w_i \mathbf{U}^{(i)} \tag{2.4}$$

where w_i is to determined such that $\mathbf{\Phi}$ maximizes Equation (2.1). The second step is useful when the number of degrees of freedom required to describe $\mathbf{U}^{(i)}$ is larger than the number of snapshots N. If Equations (2.2) and (2.4) are introduced into Equation (2.3), we have

$$\mathbf{CW} = \lambda \mathbf{W}$$

where

$$\mathbf{C}_{i,j} = \frac{1}{N} \int_{\Omega} \mathbf{U}^{(i)}(\mathbf{x}) \mathbf{U}^{(j)}(\mathbf{x})\, d\mathbf{x} \quad \text{and} \quad \mathbf{W} = \begin{bmatrix} w_1 \\ w_2 \\ \vdots \\ w_N \end{bmatrix}$$

It follows from the fact that $\mathbf{C}$ is a non-negative Hermitian matrix, in that it has a complete set of orthogonal eigenvectors

$$\mathbf{W}_1 = \begin{bmatrix} w_1^1 \\ w_2^1 \\ \vdots \\ w_N^1 \end{bmatrix}, \quad \mathbf{W}_2 = \begin{bmatrix} w_1^2 \\ w_2^2 \\ \vdots \\ w_N^2 \end{bmatrix}, \quad \ldots, \quad \mathbf{W}_N = \begin{bmatrix} w_1^N \\ w_2^N \\ \vdots \\ w_N^N \end{bmatrix}$$

along with a set of eigenvalues $\lambda_1 \ge \lambda_2 \ge \cdots \ge \lambda_N \ge 0$. We can now write down the solutions of Equation (2.1)

$$\Phi_1 = \sum_{i=1}^{N} w_i^1 \mathbf{U}^{(i)}, \quad \Phi_2 = \sum_{i=1}^{N} w_i^2 \mathbf{U}^{(i)}, \quad \ldots, \quad \Phi_N = \sum_{i=1}^{N} w_i^N \mathbf{U}^{(i)}$$

We also normalize these by requiring

$$(\mathbf{W}_l, \mathbf{W}_l) = \sum_{i=1}^{N} w_i^l w_i^{l*} = \frac{1}{N\lambda_l}$$

It is now easy to check

$$(\Phi_l, \Phi_m) = \begin{cases} 1 & l = m \\ 0 & l \neq m \end{cases}$$

This completes the construction of the orthonormal set $\{\Phi_1, \Phi_2, \ldots, \Phi_N\}$.

2.2. Optimality of the basis functions

Here, we state a proposition regarding the POD, whose proof can be found in Reference [17].

Proposition 2.1
Let $\mathbf{u}(\mathbf{x}, t) \in L^2((0, T) \times \Omega)$, and let $\{\mathbf{\Phi}_1, \mathbf{\Phi}_2, \ldots, \mathbf{\Phi}_N\}$ be the POD basis elements and $\{\lambda_1, \ldots, \lambda_N\}$ denote the corresponding set of eigenvalues. Let $\mathbf{u}^N$ be the projection of $\mathbf{u}$ onto $\text{span}\{\Phi_1, \Phi_2, \ldots, \Phi_N\}$ and

$$\mathbf{u}^N = \sum_{i=1}^{N} \beta_i(t)\mathbf{\Phi}_i(\mathbf{x})$$

Let $\{\Psi_i\}_{i=1}^N$, be an arbitrary orthonormal set such that

$$u^N = \sum_{i=1}^{N} \alpha_i(t)\mathbf{\Psi}_i$$

Then, the following hold:

(i) $\langle \beta_i(t)\beta_j^*(t) \rangle = \delta_{ij}\lambda_i$

(ii) For every $N_k \leq N$, $\displaystyle\sum_{i=1}^{N} \langle \beta_i(t)\beta_i^*(t) \rangle = \sum_{i=1}^{N} \lambda_i \geq \sum_{i=1}^{N} \langle \alpha_i(t)\alpha_i^*(t) \rangle$

where $\langle \cdot \rangle$ denotes ensemble averaging.

In essence, this proposition states that among all the linear combinations, the one corresponding to the POD is the best in the sense that it will capture the most kinetic energy possible in the average sense. Moreover, the coefficients β_i are uncorrelated. Thus, the claim that the POD expansion is efficient for modeling $\mathbf{u}(\mathbf{x}, t)$.

We note here that the average kinetic energy is given by

$$E = \int_\Omega \langle \mathbf{u}^N \mathbf{u}^{N*} \rangle \, \mathrm{d}x = \sum_{i=1}^{N} \langle \beta_i(t)\beta_i^*(t) \rangle = \sum_{i=1}^{N} \lambda_i$$

By utilizing the properties of the POD one can specify an energy level e to be captured and then seek $M \ll N$ such that

$$\frac{\displaystyle\sum_{i=1}^{M} \lambda_i}{\displaystyle\sum_{i=1}^{N} \lambda_i} > e$$

Then the POD reduced basis sub-space is defined as $\mathbf{V}^{\text{POD}} = \text{span}\{\Phi_1, \Phi_2, \ldots, \Phi_M\}$.

3. NUMERICAL SIMULATION OF A CHANNEL FLOW

In this section we will present numerical simulations for flow past a backward-facing step channel using the finite element method and using the POD reduced-order model. In particular, we will demonstrate the effectiveness of the POD reduced-order model in simulations.

3.1. Finite element simulations

We consider two-dimensional viscous incompressible flow modeled by the Navier–Stokes equations (*uncontrolled system* (S_u)) given by

$$\mathbf{u}_t - \frac{1}{Re}\Delta\mathbf{u} + \mathbf{u}\cdot\nabla\mathbf{u} + \nabla p = 0$$

$$\nabla\cdot\mathbf{u} = 0, \qquad \mathbf{u}(\mathbf{x}, 0) = \mathbf{u}_0(\mathbf{x}) \tag{3.1}$$

in the domain $\Omega \times [0, T]$. Here, the velocity $\mathbf{u}$, the pressure p, the time t and the spatial variable $\mathbf{x}$ are in non-dimensional form. The Reynolds number Re is defined as $Re = \rho u_{\text{ave}} L/\mu$, where ρ is the density, u_{ave} is the average inflow velocity, L is the channel height and μ is the kinematic viscosity. The geometry of the flow is given in Figure 1. At the inflow boundary, a parabolic velocity profile is prescribed, i.e., $u(x = 0, \frac{1}{2} \le y \le 1) = 24(y - \frac{1}{2})(1 - y)$, $v(x = 0, \frac{1}{2} \le y \le 1) = 0$, which produces a maximum inflow velocity of $u_{\max} = \frac{3}{2}$ and an average velocity of $u_{\text{ave}} = 1$. On the solid walls, the no-slip condition ($\mathbf{u} = 0$) is imposed. At the outflow, the pseudo stress-free condition

$$-p + \frac{1}{Re}\frac{\partial u}{\partial x} = 0 \quad \text{and} \quad \frac{\partial v}{\partial x} = 0$$

is applied. The boundary condition at the outflow boundary is not physical but is used to represent the flow in an unbounded region; see Reference [24].

3.1.1. Weak formulation. For the finite-dimensional approximation and for the subsequent reduced-order approximation, we need a weak form of the state equations (3.1). A weak form of Equations (3.1) has the form (see Reference [25] for similar problems)

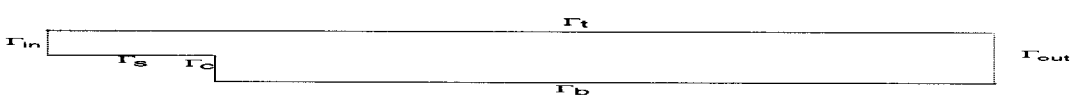

Figure 1. Computational domain for the backward-facing-step channel problem.

$$(\mathbf{u}_t + \mathbf{u}\cdot\nabla\mathbf{u}, \mathbf{v}) + \frac{1}{Re}(\nabla\mathbf{u}, \nabla\mathbf{v}) - (p, \nabla\cdot\mathbf{v}) = 0$$

$$(\nabla\cdot\mathbf{u}, q) = 0, \qquad \mathbf{u}(0) = \mathbf{u}_0 \tag{3.2}$$

for all test functions $(\mathbf{v}, q)\in\mathbf{V}\times L^2(\Omega)$, where

$$\mathbf{V} = \{\mathbf{v}\in\mathbf{H}^1(\Omega):\ \mathbf{v}\big|_{\Gamma\setminus\Gamma_{\text{out}}} = 0\}$$

The state variables $(\mathbf{u}, p)$ for the problem are taken to be

$$\mathbf{u}\in L^2(0, T;\ \mathbf{H}^1(\Omega)), \qquad \mathbf{u}\big|_{\Gamma_{\text{in}}} = \mathbf{u}_{\text{in}} \quad \text{and} \quad \mathbf{u}\big|_{\Gamma\setminus\Gamma_{\text{out}}\setminus\Gamma_{\text{in}}} = 0$$

$$p\in L^2(\Omega), \qquad \mathbf{u}_0\in L^2(\Omega), \qquad \mathbf{u}_{\text{in}}\in L^2(0, T;\ H^{1/2}(\Gamma_{\text{in}}))$$

3.1.2. Finite dimensional approximations. In this section we introduce approximations of the governing equations (3.2). We will use a finite difference scheme for time discretizations and mixed finite elements for spatial discretizations.

To discretize Equations (3.2) in time, we use a semi-implicit, first-order scheme. We denote the number of time steps by N. Let $\Delta t = T/N$, $\mathbf{u}^n = \mathbf{u}(n\Delta t)$ and $p^n = p(n\Delta t)$.

We introduce the semi-implicit time discretization as follows. For $n = 1, \ldots, N$, $(\mathbf{u}^n, p^n)\in\mathbf{H}^1\times L^2$, such that $\mathbf{u}^n\big|_{\Gamma_{\text{in}}} = \mathbf{u}_{\text{in}}$, $\mathbf{u}^n\big|_{\Gamma\setminus\Gamma_{\text{out}}\setminus\Gamma_{\text{in}}} = 0$, and

$$\left(\frac{\mathbf{u}^n - \mathbf{u}^{n-1}}{\Delta t} + \mathbf{u}^{n-1}\cdot\nabla\mathbf{u}^{n-1},\ \mathbf{v}\right) + \frac{1}{Re}(\nabla\mathbf{u}^n, \nabla\mathbf{v}) - (p^n, \nabla\cdot\mathbf{v}) = 0$$

$$(\nabla\cdot\mathbf{u}^n, q) = 0, \qquad \mathbf{u}(0) = \mathbf{u}_0 \tag{3.3}$$

for all $(\mathbf{v}, q)\in\mathbf{V}\times L^2(\Omega)$. We note here that Equations (3.3) form a linear problem in each time step as the non-linear term is treated fully explicitly.

To discretize Equations (3.2) in space, we employ a mixed finite element method. Let $\mathscr{J}^h$ be a standard finite element triangulation of Ω, where h is the maximal length of all the triangulation edges in $\mathscr{J}^h$. Denoting as $\mathscr{P}^k$ the space of all polynomials of degree less than or equal to k, and

$$\mathbf{V}^h = \{\mathbf{v}^h \big|\ \mathbf{v}^h\in C^0(\bar{\Omega})\times C^0(\bar{\Omega}),\ \mathbf{v}^h\big|_K\in\mathscr{P}^2\times\mathscr{P}^2 \quad \forall K\in\mathscr{J}^h\}$$

$$P^h = \{q^h \big|\ q^h\in C^0(\bar{\Omega}),\ g^h\big|_K\in\mathscr{P}^1 \quad \forall K\in\mathscr{J}^h\}$$

we introduce the following fully discrete approximation of Equations (3.2). For $n = 1, \ldots, N$, $(\mathbf{u}_h^n, p_h^n)$ such that $\mathbf{u}_h^n\big|_{\Gamma_{\text{in}}} = \mathbf{u}_{\text{in}}$, $\mathbf{u}_h^n\big|_{\Gamma\setminus\Gamma_{\text{out}}\setminus\Gamma_{\text{in}}} = 0$ and

$$\left(\frac{\mathbf{u}_h^n - \mathbf{u}_h^{n-1}}{\Delta t} + \mathbf{u}_h^{n-1}\cdot\nabla\mathbf{u}_h^{n-1},\ \mathbf{v}_h\right) + \frac{1}{Re}(\nabla\mathbf{u}_h^n, \nabla\mathbf{v}_h) - (p_h^n, \nabla\cdot\mathbf{v}_h) = 0$$

$$(\nabla \cdot \mathbf{u}_h^n, q_h) = 0, \qquad (\mathbf{u}_h^0, \mathbf{v}_h) = (\mathbf{u}_0, \mathbf{v}_h)$$

for all $(\mathbf{v}_h, q_h) \in \mathbf{V}^h \times P^h$. We note that the velocity and pressure are defined on the same triangulation and on each triangle the degrees of freedom for quadratic elements are the function values at the vertices and mid-points of each edge; the degrees of freedom for linear elements are the function values at the vertices. This selection satisfies the so-called inf–sup condition (see Reference [26]). We call the approximations using standard finite element basis functions, such as quadratic or linear piecewise polynomials, by 'full-order methods/discretization' and the ones using the POD by 'reduced-order methods'.

In Figure 1, the downstream channel was defined to have unit height L with a step height and inlet height $L/2$. The downstream channel length was taken as $x = 12L$. The only non-dimensional parameter of interest, the Reynolds number, is defined by $Re = u_{\text{ave}}L/v$. For comparison of channel flow simulation results, we have used the Reynolds number and problem definition used in Reference [23].

The computational grid was non-uniform in both the streamwise and cross-flow co-ordinate directions. A fine grid was used in regions where sharp variations in velocities were expected. All the computations were done with a 45×45 grid and a time step size $\Delta t = 1/200$ for the Reynolds number 200. The flow separates at the corner of the step and a recirculation forms. After the re-attachment of the lower wall eddy, the flow slowly recovers towards a fully developed Poiseuille flow. The resulting steady flow field is given in Figures 2 and 3.

To verify the grid independence of the solution, the same problem was solved by halving the grid size, i.e., using a 90×90 grid and a time step size $\Delta t' = 1/400$. The results from both grids agreed well and predicted the re-attachment point on the lower wall five step heights downstream. This re-attachment length is in agreement with the results reported in References [23,27] using a finite difference method. Typical computations require 0.02 CPU s per time step on an IBM RISC 390, while the time integration goes for 2000 time steps.

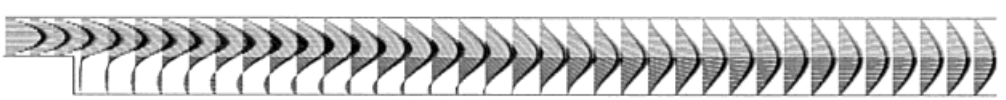

Figure 2. Baseline/uncontrolled flow; velocity field at $t = 10$.

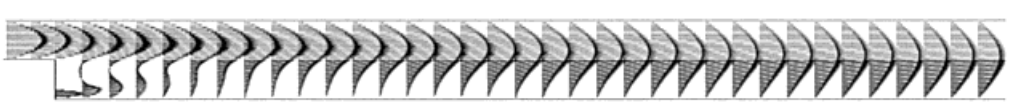

Figure 3. Controlled flow; velocity field at $t = 10$.

3.2. POD simulations

Let $\mathbf{u}(\mathbf{x}, t)$ be a given flow field and $\{\mathbf{u}(\mathbf{x}, t_k)\}_{k=1}^{N}$ be the corresponding flow fields at N different time steps t_k, i.e., the 'snapshots'. We next decompose $\mathbf{u}(\mathbf{x}, t)$ as follows:

$$\mathbf{u}(\mathbf{x}, t) = \mathbf{u}_m(\mathbf{x}) + \mathbf{v}(\mathbf{x}, t)$$

where

$$\mathbf{u}_m(x) = \frac{1}{N} \sum_{k=1}^{N} \mathbf{u}(\mathbf{x}, t_k)$$

We also define a spatial correlation matrix C with

$$C_{ij} = \frac{1}{N} \int_{\Omega} \mathbf{v}^i \mathbf{v}^j \, \mathrm{d}\mathbf{x}$$

where $\mathbf{v}^i = \mathbf{v}(\mathbf{x}, t_i)$. Then, the POD basis vectors $\mathbf{\Phi}_k$ are defined by

$$\mathbf{\Phi}_k = \sum_{i=1}^{N} w_i^k \mathbf{v}^i, \quad k = 1, \ldots, N$$

where w_i^k are the components of the eigenvector $\mathbf{W}^k$ of the eigenvalue problem

$$\mathbf{CW} = \lambda \mathbf{W}$$

The computation using the POD takes the following algorithmic form:

Algorithm I

Step 1. Solve the state equation (3.3) at N different time steps and obtain 'snapshots' $\mathscr{S}$.
Step 2. Compute the covariant matrix C. The matrix elements of C are given by

$$C_{ij} = \frac{1}{N} \int_{\Omega} \mathbf{v}^i \mathbf{v}^j \, \mathrm{d}\mathbf{x}$$

for $i, j = 1, 2, \ldots, N$.
Step 3. Solve the eigenvalue problem $\mathbf{CW} = \lambda \mathbf{W}$ for the eigenvalues and eigenvectors.
Step 4. Obtain the POD basis vectors Φ_i, $i = 1, 2, \ldots, N$, using $\Phi_i = \Sigma_{k=1}^{N} w_k^i \mathbf{v}_k$.
Step 5. Prescribe an energy level e in percentage and find $M \ll N$ such that

$$\frac{\sum_{i=1}^{M} \lambda_i}{\sum_{i=1}^{N} \lambda_i} > e$$

Step 6. Define $\mathbf{V}^{\mathrm{POD}} = \mathrm{span}\{\Phi_1, \Phi_2, \ldots, \Phi_M\}$ and expand the solution as $\mathbf{u} = \mathbf{u}_m + \Sigma_{i=1}^{M} \alpha_i(t)\Phi_i$.
Step 7. Restrict the weak form of Equations (3.2) to $\mathbf{V}^{\mathrm{POD}}$ and solve for α_i, $i = 1, 2, \ldots, N$.

3.2.1. POD reduced-order model. In this section, we consider the construction of the POD reduced-order model using a Galerkin projection of the Navier–Stokes equations onto a space spanned by the POD basis elements. The nature of the POD model is that it requires fewer basis elements than those used to approximate the flow field. In fact the first M ($\ll N$) modes carry most of the energy in the flow. Thus, one may specify an energy level e in percentage and choose M such that

$$\frac{\sum_{i=1}^{M} \lambda_i}{\sum_{i=1}^{N} \lambda_i} > e$$

and obtain a reduced-order model. In order to derive the reduced-order model, let us choose M and expand the solution as

$$\mathbf{u}(\mathbf{x}, t) = \mathbf{u}_m(\mathbf{x}) + \sum_{i=1}^{M} \alpha_i(t)\mathbf{\Phi}_i(\mathbf{x}) \tag{3.4}$$

Restriction of the weak form (3.2) to $\mathbf{V}^{\mathrm{POD}}$ results in

$$(\mathbf{u}_t + \mathbf{u}\cdot\nabla\mathbf{u}, \mathbf{\Phi}_i) - (p, \nabla\cdot\mathbf{\Phi}_i) + \frac{1}{Re}(\nabla\mathbf{u}, \nabla\mathbf{\Phi}_i) + \left(p\mathbf{n} - \frac{1}{Re}\frac{\partial\mathbf{u}}{\partial\mathbf{n}}, \mathbf{\Phi}_i\right)_{\Gamma_{\mathrm{out}}} = 0 \tag{3.5}$$

for all $\Phi_i \in \mathbf{V}^{\mathrm{POD}}$. At this point it is important to note that the POD basis elements $\mathbf{\Phi}_i$ are divergence-free, as flow is incompressible, and satisfy zero boundary conditions on $\Gamma \backslash \Gamma_{\mathrm{out}}$. Using these properties of $\mathbf{\Phi}_i$ and the boundary condition on Γ_{out}, we see that the pressure term and the boundary term vanish. Then Equation (3.5) reduces to

$$(\mathbf{u}_t + \mathbf{u}\cdot\nabla\mathbf{u}, \mathbf{\Phi}_i) + \frac{1}{Re}(\nabla\mathbf{u}, \nabla\mathbf{\Phi}_i) = 0 \tag{3.6}$$

for all $\Phi_i \in \mathbf{V}^{\mathrm{POD}}$. On substitution of Equation (3.4) into Equation (3.6) we obtain the following non-linear evolution equation for the coefficients $\boldsymbol{\alpha}(t)$:

$$\dot{\boldsymbol{\alpha}} = \mathscr{A}\boldsymbol{\alpha} + \boldsymbol{\alpha}^T\mathscr{N}\boldsymbol{\alpha} + \mathbf{e}, \qquad \boldsymbol{\alpha}(0) = \boldsymbol{\alpha}_0 \tag{3.7}$$

where

$$\mathscr{A}_{ij} = -(\boldsymbol{\Phi}_j \cdot \nabla \mathbf{u}_m, \boldsymbol{\Phi}_i) - (\mathbf{u}_m \cdot \nabla \boldsymbol{\Phi}_j, \boldsymbol{\Phi}_i) - \frac{1}{Re}(\nabla \boldsymbol{\Phi}_j, \nabla \boldsymbol{\Phi}_i), \quad i, j = 1, \ldots, M$$

$$\mathscr{N}_{ikl} = -(\boldsymbol{\Phi}_k \cdot \nabla \boldsymbol{\Phi}_l, \boldsymbol{\Phi}_i), \quad i, k, l = 1, \ldots, M$$

$$\alpha_{0i} = (\mathbf{u}_0, \Phi_i), \qquad e_i = -(\mathbf{u}_m \cdot \nabla \mathbf{u}_m, \boldsymbol{\Phi}_i) - \frac{1}{Re}(\nabla \mathbf{u}_m, \nabla \boldsymbol{\Phi}_i), \quad i = 1, \ldots, M$$

The system (3.7) is the reduced-order model of the uncontrolled system (S_u).

3.2.2. Numerical results. The 'snapshots' for the reduced-order model were obtained by simulating the uncontrolled system (S_u) in the time interval [0, 10]. One hundred 'snapshots' were recorded at constant time intervals Δt^* ($\Delta t^* = 20\Delta t$). The correlation matrix C was formed with the aid of the finite element routine and the eigenvalue solve was carried out using the RG sub-routine in the Fortran library EISPACK. The eigenvalue spectrum from the correlation matrix C is shown in Figure 4(left). As shown in the figure, the eigenvalues quickly decay and thus very few modes capture the essential energy in the flow.

The percentages of the full-order model energy captured by the POD reduced-order model are given in Table I, which indicates only nine basis functions were enough to capture 99.9 per cent of the energy of the full-order model. The reduced-order system was solved using the backward Euler method with the time step $\Delta t = 1/200$ and the resulting non-linear algebraic system was solved using the Newton iterative method. Figures 5 and 6 are the channel flow computations with 'full solution' and reduced-order solution at time $t = 10$ for various stations in the channel, which show excellent qualitative and quantitative agreement. In Table I we

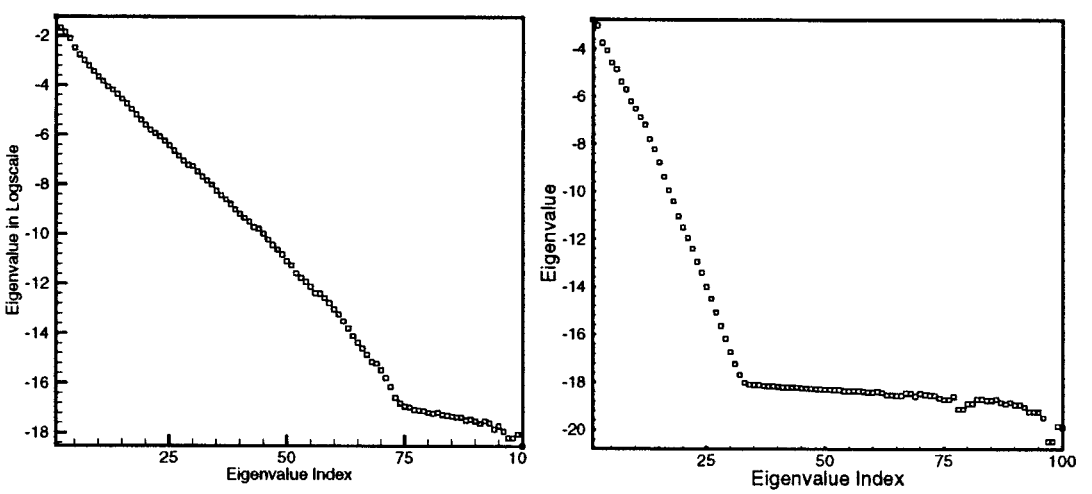

Figure 4. Eigenvalues of the correlation matrix for the baseline and controlled case respectively.

Table I. ℓ_1-norm difference between full order and POD reduced-order model solutions, condition numbers of the mass matrix and percentage of full order model energy captured with $M = 3$, 6, 9, 12, 15 and 20 POD basis functions.

M	3	6	9	12	15	20
ℓ_1 Error	0.0013	0.001	0.000769	0.000359	0.00029	0.00017
Condition no. κ	1.0	1.0	1.0	1.0	1.0	1.0
Per cent of energy	97.0	99.68	99.96	99.997	99.999	99.9999

show that the ℓ_1-norm of the difference between solutions of the POD reduced-order and full-order solutions decays as the dimension of the POD sub-space increases.

These simulations also showed good agreement at intermediate time levels. This indicates that the reduced-order model also has good short-term prediction capabilities, which are

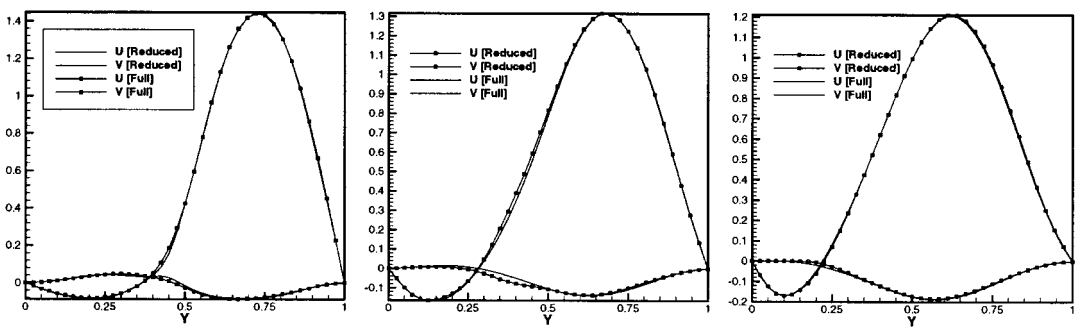

Figure 5. Comparison of full model and reduced model solutions; velocity components u and v at various stations in the channel.

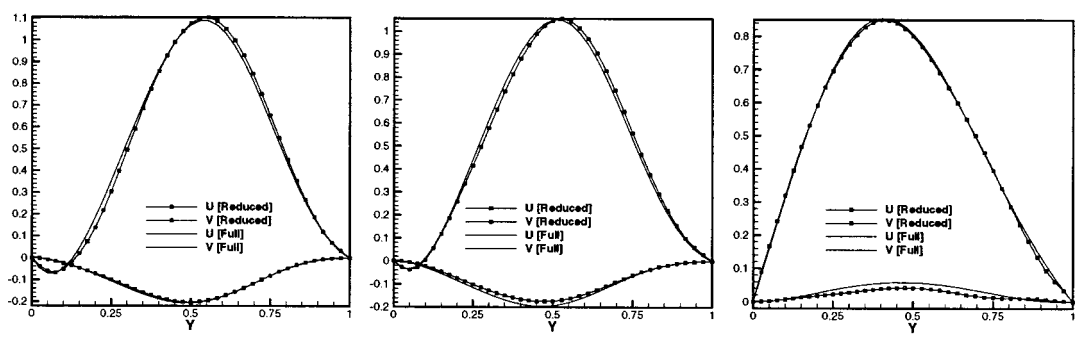

Figure 6. Comparison of full model and reduced model solutions; velocity components u and v at various stations in the channel.

essential for real-time flow control applications. We also found out, at least for the Reynolds number case studied ($Re = 200$), the use of several transients in the ensemble was not essential. A single transient ensemble also gave very good results.

In order to highlight some of the other features of the POD reduced-order model, let us next compare it with another reduced-order model based on the so-called *reduced basis method* (RBM); see Reference [3]. In Reference [3] several ways to choose reduced basis sub-spaces are discussed. Here, we consider the so-called Lagrange sub-space. The basis elements in the Lagrange sub-space are snapshots of the problem obtained by solving system (3.1) using a full-order method. Supposing $\{\Psi_i\}_{i=1}^{M+1}$ denotes the snapshots, the reduced-order sub-space is defined as $V^{\mathrm{RBM}} = \mathrm{span}\{\Phi_i\}_{i=1}^{M} = \mathrm{span}\{\Psi_{i+1} - \Psi_i\}_{i=1}^{M}$ and the reduced-order solution is defined as $\mathbf{u} = \Psi_{M+1} + \Sigma_{i=1}^{M} \alpha_i \Phi_i$. Once we have a reduced-order sub-space V^{RBM}, system (3.1) is projected onto V^{RBM} to obtain a reduced-order model as in Section 3.4.

In algorithmic form, the RBM can be summarized in the following form:

Algorithm 2

Step 1. Solve the state equation (3.3) at $M+1$ different time steps and obtain 'snapshots' $\mathscr{S} = \{\Psi_i\}_{i=1}^{M+1}$.
Step 2. Define $\mathbf{V}^{\mathrm{RBM}} = \mathrm{span}\{\Phi_i\}_{i=1}^{M} = \mathrm{span}\{\Psi_{i+1} - \Psi_i\}_{i=1}^{M}$ and seek the solutions as $\mathbf{u} = \Psi_{M+1} + \Sigma_{i=1}^{M} \alpha_i(t)\Phi_i$, where Ψ_{M+1} account for the non-zero boundary values.
Step 3. Restrict the weak form (3.2) to $\mathbf{V}^{\mathrm{RBM}}$ and solve for α_i, $i = 1, 2, \ldots, M$.

For the RBM simulations, we considered the channel flow problem described earlier. The 'snapshots' were obtained from the finite element simulations in the time interval [0, 10]. Eleven 'snapshots' were recorded at constant time intervals Δt^* ($\Delta t^* = 200\Delta t$). In other words, we simply take fewer 'snapshots' and apply Galerkin projection to obtain the RBM reduced-order model. The reduced-order model simulations here used the same data as in the POD reduced-order model simulations. In order to see whether the reduced-order approximation becomes more accurate as the dimension increases we computed the ℓ_1-norm of the difference between the reduced-order and full-order solutions. In Table II we present the ℓ_1-norm error using $M = 3$, 6 and 9 basis functions. We also report the condition numbers of the resulting mass matrices. As seen, the condition number can increase dramatically with increasing basis elements deteriorating convergence. However, the POD reduced-order model does not generate

Table II. ℓ_1-norm difference between full order and RBM reduced-order model solutions and condition numbers of the mass matrix, with $M = 3$, 6 and 9 basis functions.

M	3	6	9
ℓ_1 Error	0.0327	0.0057	0.0035
Condition no. κ	599.87	10 220.09	144 662.92

such bad condition numbers as seen in Table I. Moreover, the POD allows easy generation of linearly independent basis elements and more stable system matrices.

4. POD FOR OPTIMAL CONTROL OF FLUIDS

Minimization of the vorticity level in a flow domain is of interest in the control/delay of the transition of flow past bluff bodies. Thus, in this section we formulate a related optimal control problem in channel flow. The flow configuration considered is a backward-facing step channel. As the Reynolds number is increased, the flow separates near the corner of the step. The objective of the optimal control is to reduce the size of the recirculation and hence of the length of re-attachment. The control action is effected through blowing on Γ_c. In terms of boundary condition it takes the following form along the boundary Γ_c

$$\mathbf{u} = c(t)\mathbf{g}(\mathbf{x}) \quad \text{on } \Gamma_c \times [0, T]$$

where $c(t)$: $[0, T] \to \mathbb{R}$ and $\mathbf{g}(\mathbf{x})$ represent respectively the temporal dependence and spatial distribution of the fluid velocity on the boundary Γ_c; see Reference [6]. The *controlled system* (S_c) we consider is

$$\mathbf{u}_t - \frac{1}{Re}\Delta\mathbf{u} + \mathbf{u}\cdot\nabla\mathbf{u} + \nabla p = 0$$

$$\nabla\cdot\mathbf{u} = 0, \qquad \mathbf{u}(\mathbf{x}, 0) = \mathbf{u}_0(\mathbf{x})$$

in the domain $\Omega \times [0, T]$ and the following boundary conditions:

$$\begin{aligned}
&\mathbf{u} = (24(y - 1/2)(1 - y), 0) && \text{on } \Gamma_{\text{in}} \times [0, T]\\
&p\mathbf{n} - \frac{1}{Re}\frac{\partial\mathbf{u}}{\partial n} = (0, 0) && \text{on } \Gamma_{\text{out}} \times [0, T]\\
&\mathbf{u} = c(t)\mathbf{g}(\mathbf{x}) && \text{on } \Gamma_c \times [0, T]\\
&\mathbf{u} = (0, 0) && \text{on } \Gamma_t \cup \Gamma_b \cup \Gamma_s \times [0, T]
\end{aligned}$$

The choice of cost functional or objective functional to meet the control objective of reducing the recirculation is not trivial. Here we will consider a functional of the form

$$\mathscr{G}(\mathbf{u}) = \int_\Omega |\nabla \times \mathbf{u}|^2 \, d\mathbf{x}$$

which corresponds to minimization of vorticity levels in the flow. The task is to find $c(t)$ such that the cost functional

$$\mathscr{J}(\mathbf{u}, U) = \frac{1}{2}\int_0^T [\mathscr{G}(\mathbf{u}) + \beta |U|^2]\, \mathrm{d}t$$

is minimized subject to the constraint that the flow fields satisfy the controlled system (S_c). By including a term involving U one minimizes the rate of change of control velocity. The parameter $\beta > 0$ adjusts the relative weight of the two terms in the functional.

In order to obtain an ensemble of data for the controlled system (S_c) one cannot continue to use the 'snapshots' of the uncontrolled system (S_u). To obtain 'snapshots' for the controlled system we take 'snapshots' with a specified control input (not necessarily optimal). In our subsequent calculations, for example, we introduce

$$\mathbf{u}_c(\mathbf{x}) = (\mathbf{u}_{c_1}(\mathbf{x}) - \mathbf{u}_{c_0}(\mathbf{x}))/(c_1 - c_0)$$

where $\mathbf{u}_{c_1}$ is a steady flow with $c(t) = c_1 = 10$ on Γ_c and $\mathbf{u}_{c_0}$ is that with $c(t) = c_0 = 0$ on Γ_c. Then the 'snapshots' are defined as

$$\mathbf{u}(\mathbf{x}, t_k) - c(t_k)\mathbf{u}_c(\mathbf{x})$$

and the basis functions $\mathbf{\Phi}_j$ as defined in Algorithm 1 have zero boundary conditions on the Dirichlet boundaries. The velocity expansion is defined as

$$\mathbf{u}(\mathbf{x}, t) = \mathbf{u}_m(\mathbf{x}) + c(t)\mathbf{u}_c(\mathbf{x}) + \sum_{i=1}^{M} \boldsymbol{\alpha}_i(t)\mathbf{\Phi}_i(\mathbf{x}) = \mathbf{\Phi}_0(\mathbf{x}) + c(t)\mathbf{\Phi}_{M+1}(\mathbf{x}) + \sum_{i=1}^{M} \boldsymbol{\alpha}_i(t)\mathbf{\Phi}_i(\mathbf{x}) \qquad (4.1)$$

so as to automatically satisfy all the Dirichlet boundary conditions.

4.1. The reduced-order control problem

The reduced-order control system derivation is similar to that of the uncontrolled system in Section 3.2.1. Inserting the expansion (4.1) into the Galerkin projection of the Navier–Stokes equations, we obtain

$$\dot{\boldsymbol{\alpha}} + A\mathbf{X} + \mathbf{X}^T \mathscr{N} \mathbf{X} - BU = 0, \qquad \boldsymbol{\alpha}(0) = \boldsymbol{\alpha}_0 \qquad (4.2)$$

where $\mathbf{X} = (1, \boldsymbol{\alpha}, C)^T$, U is the control, and we define the vector B, the stiffness matrix A and the initial condition $\boldsymbol{\alpha}_0$ as follows:

$$B_i = -(\mathbf{u}_c, \mathbf{\Phi}_i), \quad i = 1, \ldots, M$$

$$\mathscr{A}_{ij} = \frac{1}{Re}(\nabla\mathbf{\Phi}_i, \nabla\mathbf{\Phi}_j), \quad i = 1, \ldots, M, \quad j = 1, \ldots, M+1$$

$$\alpha_{0i} = (\mathbf{u}_0, \Phi_i), \quad i = 1, \ldots, M$$

where $\mathbf{u}_0$ is the initial condition. Moreover, $(\mathbf{X}^T\mathscr{N}\mathbf{X})_i = \mathbf{X}^T\mathscr{P}_i\mathbf{X}$, $i = 1, \ldots, M$, and

$$(\mathscr{P}_i)_{kl} = (\boldsymbol{\Phi}_k \cdot \nabla\boldsymbol{\Phi}_l, \boldsymbol{\Phi}_i), \quad i = 1, \ldots, M, \quad k, l = 1, \ldots, M+1$$

The resulting reduced-order control system is

$$\dot{\mathbf{X}} = f(\mathbf{X}) + BU, \qquad \mathbf{X}(0) = \mathbf{X}_0 \tag{4.3}$$

where

$$f(\mathbf{X}) = -\mathbf{A}\mathbf{X} - \mathbf{N}(\mathbf{X})$$

Similarly from the cost functional $\mathscr{J}$, we obtain

$$\mathscr{J}(\mathbf{X}, U) = \int_0^T \left[\ell(\mathbf{X}) + \frac{\beta}{2}U^2\right] \mathrm{d}t \tag{4.4}$$

where

$$\ell(\mathbf{X}) = \frac{1}{2}\mathbf{X}^T\mathscr{Q}\mathbf{X}, \qquad \mathscr{Q}_{i,j} = (\nabla \times \boldsymbol{\phi}_i, \nabla \times \boldsymbol{\phi}_j), \quad i, j = 0, \ldots, M+1$$

The optimal control problem we consider is

Find U that minimizes $\mathscr{J}(\mathbf{X}, U)$ *subject to* (4.3).

At this point one can employ a variety of numerical methods designed for finite-dimensional non-linear optimal control problems, such as multiple shooting methods. Our method here is based on Newton's method for the necessary condition of optimality or the so-called optimality system

$$\left.\begin{aligned} \dot{\mathbf{X}}(t) &= F(\mathbf{X}(t)) - \frac{1}{\beta}BB^T\boldsymbol{\zeta}(t), \quad \mathbf{X}(0) = \mathbf{X}_0 \\ -\dot{\boldsymbol{\zeta}} &= F_{\mathbf{X}}(\mathbf{X})^T\boldsymbol{\zeta}(t) + \ell_{\mathbf{X}}(\mathbf{X}), \qquad \boldsymbol{\zeta}(T) = 0 \end{aligned}\right\} \tag{4.5}$$

where $\boldsymbol{\zeta}$ is the adjoint variable or the Lagrange multiplier. We further remark here that finite-dimensional control systems like the one given above can also be obtained using, for example, the finite element method as in Section 3. However, their size is too large for practical control systems, whereas the POD-based reduced-order control systems are low-order and maintain high fidelity. This makes our approach extremely attractive for optimal control problems governed by PDEs.

4.2. Approximation of the reduced-order control problem

In what follows we describe a general procedure for solving the two-point boundary value problem (4.5). Instead of the direct approximation of (4.5), we will approximate (4.3) and (4.4) using the Crank–Nicholson method for the constraint and the trapezoidal rule for the cost functional. We obtain

$$\text{Minimize } \mathscr{J}^N = \sum_{k=1}^{N} \left[\frac{1}{2} (\ell(\mathbf{X}^{k-1}) + \ell(\mathbf{X}^k)) + h(U^k) \right] \Delta t \tag{4.6}$$

subject to

$$\frac{\mathbf{X}^k - \mathbf{X}^{k-1}}{\Delta t} = \frac{1}{2} (f(\mathbf{X}^k) + f(\mathbf{X}^{k-1})) + BU^k, \quad k = 1, \ldots, N \tag{4.7}$$

where $N\,\Delta t = T$ and $\mathbf{X}^0 = \mathbf{X}_0$. The necessary optimality condition for (4.6) and (4.7) is given by

$$\left.\begin{aligned} \frac{\mathbf{X}^k - \mathbf{X}^{k-1}}{\Delta t} &= \frac{1}{2} (f(\mathbf{X}^k) + f(\mathbf{X}^{k-1})) - \frac{1}{\beta} BB^T \zeta^k \\ -\frac{\zeta^{k+1} - \zeta^k}{\Delta t} &= \frac{1}{2} f_{\mathbf{X}}(\mathbf{X}^k)^T (\zeta^k + \zeta^{k+1}) + \ell_{\mathbf{X}}(\mathbf{X}^k) \end{aligned}\right\} \tag{4.8}$$

for $k = 1, \ldots, N$ and $\mathbf{X}^0 = \mathbf{X}_0$ and $\zeta^{N+1} = 0$, and the optimal control to Equations (4.6) and (4.7) is given by

$$U^k = -\frac{1}{\beta} B^T \zeta^k \tag{4.9}$$

System (4.8)–(4.9), which is an approximation of Equation (4.5), is a sparse system of non-linear equations in $\mathbf{X}^k$, ζ^k and can be solved using Newton's method

$$\mathscr{F}'(\mathbf{Y}^-)(\mathbf{Y}^+ - \mathbf{Y}^-) = \mathscr{F}(\mathbf{Y}^-)$$

where $\mathbf{Y} = (\mathbf{X}^1, \mathbf{X}^2, \ldots, \mathbf{X}^N, \zeta^1, \zeta^2, \ldots, \zeta^N)$

$$\mathscr{F}(\mathbf{Y}) = \begin{bmatrix} \dfrac{\mathbf{X}^k - \mathbf{X}^{k-1}}{\Delta t} - \dfrac{1}{2} (f(\mathbf{X}^k) + f(\mathbf{X}^{k-1})) + \dfrac{1}{\beta} BB^T \zeta^k \\ \dfrac{\zeta^{k+1} - \zeta^k}{\Delta t} + \dfrac{1}{2} f_{\mathbf{X}}(\mathbf{X}^T)(\zeta^k + \zeta^{k+1}) + \ell_{\mathbf{X}}(\mathbf{X}^k) \end{bmatrix}$$

and the Jacobian has the following form:

$$\mathscr{F}' = \begin{bmatrix} A & S \\ Q & -A^T \end{bmatrix}$$

where A is block lower bi-diagonal, and S and Q are block diagonal with block size M. The diagonal and sub-diagonal blocks of A are given by

$$A_{k,k} = \frac{I}{\Delta t} + \frac{1}{2} f_{\mathbf{X}}(\mathbf{X}^k) \quad \text{and} \quad A_{k+1,k} = -\frac{I}{\Delta t} + \frac{1}{2} f_{\mathbf{X}}(\mathbf{X}^k)$$

The block S is the constant

$$S_{k,k} = \frac{1}{\beta} B^T B$$

and the diagonal block Q is given by

$$Q_{k,k} = \ell_{\mathbf{XX}}(\mathbf{X}^k) + \frac{1}{2} f_{\mathbf{X},\mathbf{X}}(\mathbf{X}^k)^T(\zeta^k + \zeta^{k+1})$$

We note here that the vector $\mathbf{Y} = (\mathbf{X}^1, \mathbf{X}^2, \ldots, \mathbf{X}^N, \zeta^1, \zeta^2 \ldots, \zeta^N)^T$ is rearranged to

$$\mathbf{Y} = (\mathbf{X}^1, \zeta^1, \mathbf{X}^2, \zeta^2, \ldots, \mathbf{X}^N, \zeta^N)$$

then each Newton step can be solved using a block tridiagonal algorithm.

4.3. Computational results

Here we present numerical results for the POD based control and compare its performance with that of RBM. The flow configuration is chosen as the two-dimensional backward-facing step. The control objective is to reduce the recirculation behind the step and thus the re-attachment length. The cost functional is taken to be the vorticity functional defined earlier.

The control is effected through blowing on the lower quarter of the boundary Γ_c, Thus, we consider

$$\mathbf{u} = \begin{cases} c(t)\mathbf{g}(\mathbf{x}) & \text{on } 0 \le y \le \frac{1}{8} \\ 0 & \text{on } \frac{1}{8} < y \le \frac{1}{2} \end{cases}$$

and $\mathbf{g}(\mathbf{x}) = (30y(\frac{1}{8} - y), 0)$. The portion of the boundary Γ_c , where control is applied, is the line segment between $y = 0$ and $y = 0.125$ at $x = 0.5$. This choice here is motivated by the fact that if one wants maximum influence in the flow, then the control has to be applied in that vicinity.

4.3.1. Test I (POD). We present numerical results for the POD approach in solving the optimal control problem at $Re = 200$. Recall that the control problem we consider is

$$\text{Minimize } \mathscr{J}(\mathbf{u}, U) = \frac{1}{2}\int_0^T [\mathscr{G}(u) + \beta|U|^2]\,\mathrm{d}t$$

subject to

$$(\mathbf{u}_t + \mathbf{u}\cdot\nabla\mathbf{u}, \Phi_i) + \frac{1}{Re}(\nabla\mathbf{u}, \nabla\Phi_i) = 0, \quad i = 1, \ldots, M$$

where M is the number of POD modes and

$$\mathbf{u} = \mathbf{u}_m + c(t)\mathbf{u}_c + \sum_{i=1}^{M} \alpha_i(t)\Phi_i(\mathbf{x})$$

The 'snapshots' for the reduced-order control system were obtained by employing a given linear profile for $c(t) = t$ and simulating the system (S_c) in the interval [0, 10]. A hundred 'snapshots' were recorded at constant time intervals Δt^* ($\Delta t^* = 20\Delta t$). The eigenvalues of the correlation matrix decay rapidly (Figure 4(right)). The initial state and control were given prescribed values and the optimal control problem was solved using the algorithm described in Section 4.2.

We carried out several simulations to study the performance of the controller. Here we present only a sample of the results. The penalty parameter β was found to play a critical role in the controller design. For $\beta \leq 1$ control oscillates at the beginning and the end of the time interval. The amplitude of the oscillation increases as more weight is placed on achieving the vorticity reduction by decreasing the parameter value β in the cost functional $\mathscr{J}$. In other words, oscillations increases as the rate of change of control U is increased (Figure 9), whereas for $\beta \geq 50$, control undershoots. With the values $\beta = 20$, a smooth control was obtained.

The controlled flow fields with four, nine and 14 modes showed similar results and hence only results with nine modes are presented. The flow fields presented in Figures 7 and 8 are u components of the flow field $\mathbf{u}$ at different stations in the channel for the controlled and uncontrolled cases with nine POD modes. As indicated by the controlled flow fields, separation has been effectively eliminated by the optimal blowing control. Significant reduction in the recirculation bubble is seen. The re-attachment length has been reduced by more than 90 per cent compared with the uncontrolled case.

4.3.2. Test II (RBM). We next present numerical results for the RBM approach. The reduced-order solution is defined as

$$\mathbf{u} = \Phi_0 + c(t)\Phi_{M+1} + \sum_{i=1}^{M} \alpha_i(t)\Phi_i$$

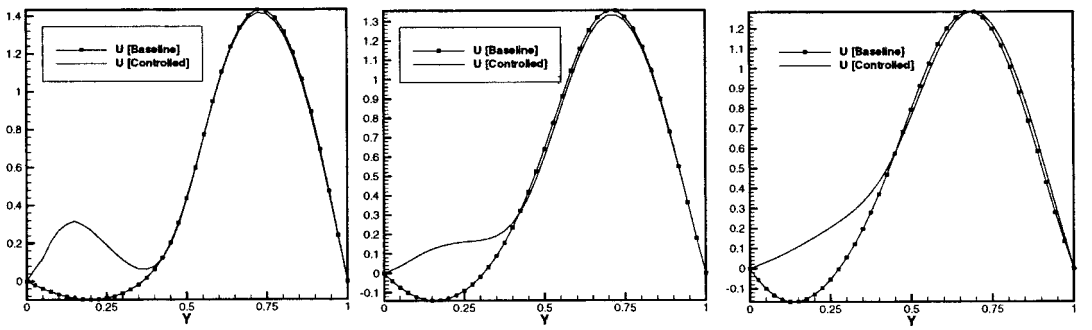

Figure 7. The controlled and uncontrolled flow: u component velocity field.

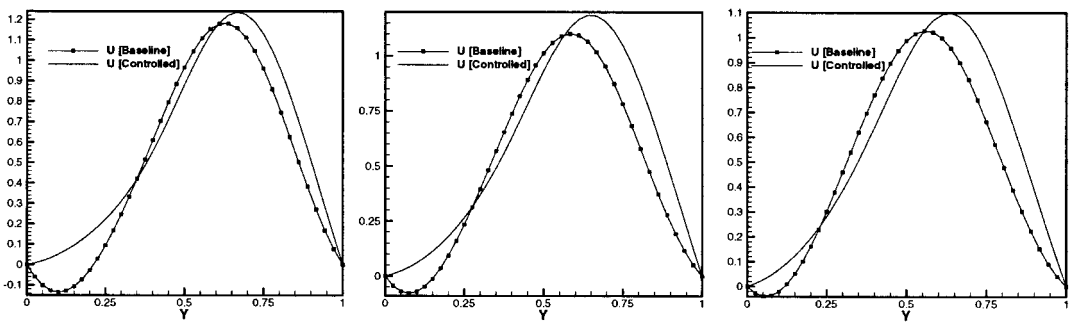

Figure 8. The controlled and uncontrolled flow: u component of the velocity field.

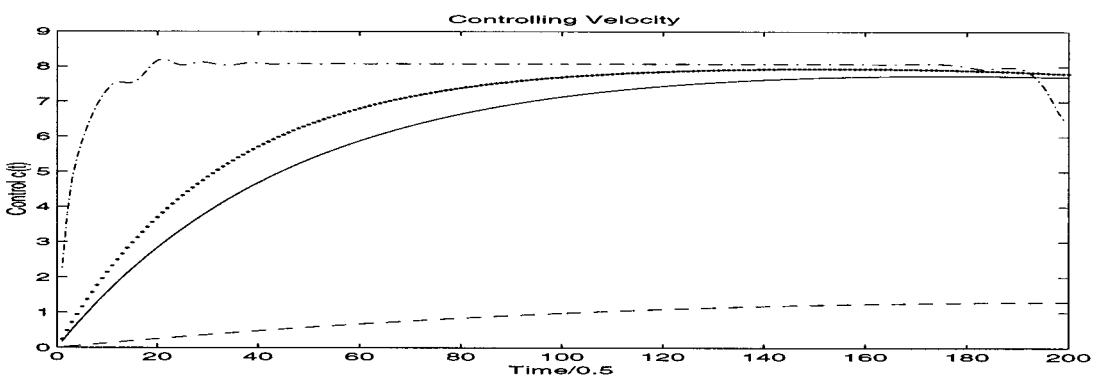

Figure 9. Optimal control (POD) as function of non-dimensional time for different values of β: 1000 (dashed line), 20 (line), 10 (dotted line), 0.1 (dashed–dot line).

where the test functions Φ_i, $i = 1, \ldots, M$ are defined such that they are zero on all the Dirichlet boundaries. The trial function Φ_0 denotes a flow corresponding to a zero control and Φ_{M+1} denotes a flow corresponding to non-zero values on the control part of the boundary Γ_c. In the calculation we obtained Φ_i values as follows. First M 'snapshots' were recorded at constant time intervals Δt^* $(= 200\Delta t)$ with a prescribed linear profile $c(t) = t$ in the time interval [0, 10]. Then the test functions were defined as follows:

$$\mathbf{\Phi}_0 = \mathbf{u}_{c_0}$$

$$\mathbf{\Phi}_k = \mathbf{u}(\mathbf{x}, t_k) - c(t_k)\mathbf{u}_c - \mathbf{u}_{c_0}, \quad k = 1, \ldots, M$$

$$\mathbf{\Phi}_{M+1} = \mathbf{u}_c$$

The time interval [0, T], the time step Δt and the other data were all taken the same as in the previous case.

We repeated the parameter study on the penalty parameter β to verify the findings in the previous test. The results are presented in Figure 10, which show similar behavior. As in the previous test, the oscillations increase as the rate of change of control U is increased. Whereas, for $\beta \geq 50$, control undershoots. With the values $\beta = 20$, a smooth control was obtained.

The control distribution presented in Figure 10 and the controlled flow fields (not presented here) all agree well with that of POD. This shows the ability of RBM to provide very good controls with very few elements. However, RBM can be sensitive in terms of condition numbers of the system matrices as one increases the number of basis functions in order to improve convergence and accuracy.

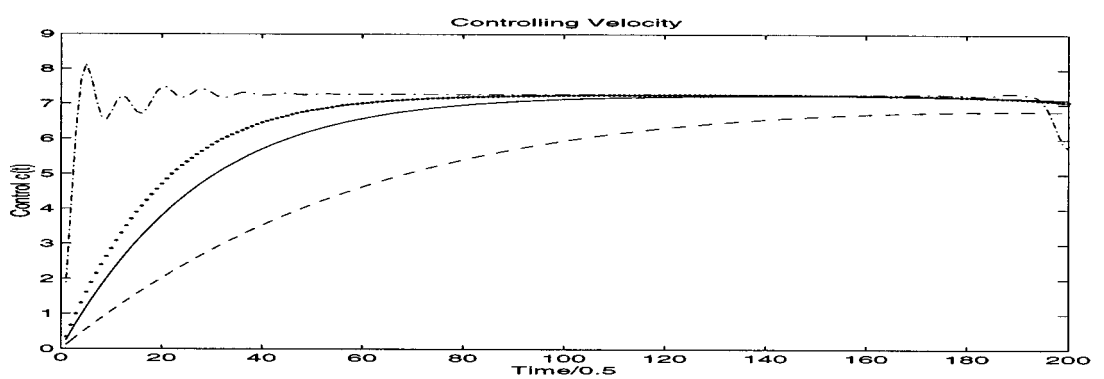

Figure 10. Optimal control (RBM) as function of non-dimensional time for different values of β: 100 (dashed line), 20 (line), 10 (dotted line), 0.1 (dashed–dot line).

5. CONCLUSION

In this article we have presented a reduced-order modeling approach for optimal control of fluid flows. A reduced-order model suitable for control and which captures the essential physics was developed using the POD. We have shown two different ways to define the 'snapshots': (i) solutions to the uncontrolled system at various time instances, (ii) solutions to the controlled system with varying boundary control input. The former is used only for simulation of the uncontrolled system as it may not produce a reduced-order model that is representative of the control system. However, the latter approach leads more naturally to the reduced-order control problem. Our computational investigations into the use of reduced-order methods for control suggest promise. Significant computational savings were evidenced in the test cases considered. In the RBM there is no systematic way to increase the level of accuracy, and ill-conditioned system matrices can make it impossible to improve the accuracy, whereas the POD provides a systematic way to improve the level of accuracy while maintaining well-conditioned system matrices. However, even the POD may fail to effectively represent the dynamics of the system as it merely provides an efficient way to represent the energy in the ensemble data set. Whenever they can be effective they can provide significant performance with substantially lower on-line computational resources.

ACKNOWLEDGMENTS

This work was supported in part by the National Aeronautics and Space Administration under NASA Contract NASW-8154.

REFERENCES

1. Hou LS, Ravindran SS. A penalized Neumann control approach for solving an optimal Dirichlet control problem for the Navier–Stokes equations. *SIAM Journal on Control and Optimization* 1997; **36**(5): 1795–1814.
2. Hou LS, Ravindran SS. Computations of boundary optimal control problems for an electrically conducting fluid. *Journal of Computational Physics* 1996; **128**(2): 319–330.
3. Ito K, Ravindran SS. A reduced order method for simulation and control of fluid flows. *Journal of Computational Physics* 1998; **143**: 403–425.
4. Joslin RD, Gunzburger MD, Nicolaides R, Erlebacher G, Hussaini MY. A self-contained, automated methodology for optimal flow control validated for transition delay. *AIAA Journal* 1997; **35**: 816–824.
5. Ou YR. Design of feedback compensators for viscous flow. In *Optimal Control of Viscous Flow*, Sritharan SS (ed.). SIAM: Philadelphia, PA, 1998; 151–180.
6. Sritharan SS. Dynamic programming of the Navier–Stokes equations. *System and Control Letters* 1991; **16**: 299–307.
7. Seifert A, Darabi A, Wyganski I. Delay of airfoil stall by periodic excitation. *Journal of Aircraft* 1996; **33**(4): 691–698.
8. Smith BL, Glezer A. Vectoring and small scale motions effected in free shear flows using synthetic jet actuators. AIAA Paper No. 97-0213, 1997.
9. Modi J, Mokhtarian F, Fernando M, Yokomizo T. Moving surface boundary-layer control as applied to two-dimensional airfoils. *Journal of Aircraft* 1991; **28**: 104–112.
10. Maddalon V, Collier FS, Montoya FS, Land CK. Transition flight experiments on a swept wing with suction. AIAA Paper No. 89-1893, 1989.
11. Roussopoulos K. Feedback control of vortex shedding at low Reynolds numbers. *Journal of Fluid Mechanics* 1993; **248**: 267–296.
12. Karhunen K. Zur spektral theorie stochasticher prozesse. *Ann Acad Sci Fennicae*, *Ser A1 Math Phys* 1946; **34**: 1–7.

13. Loeve M. Functiona aleatoire de second ordre. *Revue Science* 1946; **84**: 195–206.
14. Lumley JL. The structure of inhomogeneous turbulence. In *Atmospheric Turbulence and Radio Wave Propagation*, Yaglom AM, Tatarski VA (eds). Nauka: Moscow, 1967; 166–178.
15. Sirovich L. Turbulence and the dynamics of coherent structures: part I–III. *Quarterly of Applied Mathematics* 1987; **45**(3): 561–590.
16. Aubry N, Holmes P, Lumley JL, Stone E. The dynamics of coherent structures in the wall region of a turbulent boundary layer. *Journal of Fluid Mechanics* 1988; **192**: 115–173.
17. Berkooz G, Holmes P, Lumley JL. The proper orthogonal decomposition in the analysis of turbulent flows. *Annual Review of Fluid Mechanics* 1993; **25**(5): 539–575.
18. Ball KS, Sirovich L, Keefe LR. Dynamical eigenfunction decomposition of turbulent channel flow. *International Journal for Numerical Methods in Fluids* 1991; **12**: 585–604.
19. Kirby M, Boris JP, Sirovich L. A proper orthogonal decomposition of a simulated supersonic shear layer. *International Journal for Numerical Methods in Fluids* 1990; **10**: 411–428.
20. Moin P, Moser RD. Characteristic-eddy decomposition of turbulence in a channel. *Journal of Fluid Mechanics* 1989; **200**: 417–509.
21. Rajaee M, Karlson SKF, Sirovich L. Low-dimensional description of free shear flow coherent structures and their dynamical behavior. *Journal of Fluid Mechanics* 1994; **258**: 1401–1402.
22. Sirovich L. Analysis of turbulent flows by means of the empirical eigenfunctions. *Fluid Dynamics Research* 1991; **8**: 85–100.
23. Armaly BF, Durst F, Pereira JCF. Experimental and theoretical investigation of backward-facing step flow. *Journal of Fluid Mechanics* 1983; **127**: 473–496.
24. Sani RL, Gresho PM. Resume and remarks on the open boundary condition mini-symposium. *International Journal of Numerical Methods in Fluids* 1994; **18**: 983–1008.
25. Temam R. *Navier–Stokes Equations and Nonlinear Functional Analysis*. SIAM: Philadelphia, PA, 1983.
26. Gunzburger D. *Finite Element Methods for Viscous Incompressible Flows*. Academic Press: London, 1989.
27. Kim J, Moin P. Application of a fractional-step method to incompressible Navier–Stokes equations. *Journal of Computational Physics* 1985; **59**: 308–323.
28. Park DS, Ladd DM, Hendricks EW. Feedback control of Kármán vortex shedding. In *Symposium on Active Control of Noise and Vibration*, 19th ASME Winter Annual Meeting, Anaheim, CA, 1992.

